

Review

Recent Advances in g-C₃N₄ Photocatalysts: A Review of Reaction Parameters, Structure Design and Exfoliation Methods

Junxiang Pei, Haofeng Li, Songlin Zhuang, Dawei Zhang and Dechao Yu *

Engineering Research Center of Optical Instrument and System, Ministry of Education and Shanghai Key Laboratory of Modern Optical System, University of Shanghai for Science and Technology, Shanghai 200093, China; jxpei@usst.edu.cn (J.P.); lhf09042023@163.com (H.L.); slzhuangx@aliyun.com (S.Z.); dwzhang@usst.edu.cn (D.Z.)

* Correspondence: d.yu@usst.edu.cn

Abstract: Graphitized carbon nitride (g-C₃N₄), as a metal-free, visible-light-responsive photocatalyst, has a very broad application prospect in the fields of solar energy conversion and environmental remediation. The g-C₃N₄ photocatalyst owns a series of conspicuous characteristics, such as very suitable band structure, strong physicochemical stability, abundant reserves, low cost, etc. Research on the g-C₃N₄ or g-C₃N₄-based photocatalysts for real applications has become a competitive hot topic and a frontier area with thousands of publications over the past 17 years. In this paper, we carefully reviewed the recent advances in the synthesis and structural design of g-C₃N₄ materials for efficient photocatalysts. First, the crucial synthesis parameters of g-C₃N₄ were fully discussed, including the categories of g-C₃N₄ precursors, reaction temperature, reaction atmosphere and reaction duration. Second, the construction approaches of various nanostructures were surveyed in detail, such as hard and soft template, supramolecular preorganization and template-free approaches. Third, the characteristics of different exfoliation methods were compared and summarized. At the end, the problems of g-C₃N₄ materials in photocatalysis and the prospect of further development were disclosed and proposed to provide some key guidance for designing more efficient and applicable g-C₃N₄ or g-C₃N₄-based photocatalysts.

Keywords: photocatalyst; g-C₃N₄; reaction parameters; structure design; exfoliation



Citation: Pei, J.; Li, H.; Zhuang, S.; Zhang, D.; Yu, D. Recent Advances in g-C₃N₄ Photocatalysts: A Review of Reaction Parameters, Structure Design and Exfoliation Methods. *Catalysts* **2023**, *13*, 1402. <https://doi.org/10.3390/catal13111402>

Academic Editors: Weilong Shi, Feng Guo, Xue Lin and Yuanzhi Hong

Received: 7 October 2023

Revised: 25 October 2023

Accepted: 26 October 2023

Published: 28 October 2023



Copyright: © 2023 by the authors. Licensee MDPI, Basel, Switzerland. This article is an open access article distributed under the terms and conditions of the Creative Commons Attribution (CC BY) license (<https://creativecommons.org/licenses/by/4.0/>).

1. Introduction

In order to alleviate the problem of global warming and energy shortage, the development of renewable energy has become a major practical problem to be urgently solved by researchers all over the world [1]. As the most important renewable energy on the Earth, solar energy can be said to be inexhaustible. But so far, limited by various energy conversion technologies, the development and utilization of solar energy in the field of photocatalysis is far from enough. Recently, graphitic carbon nitride (g-C₃N₄) has attracted extremely wide attentions in photocatalysis due to its special band structure, stable properties, low price, and easy preparation [2–6]. The g-C₃N₄ is comprised of only carbon and nitrogen elements, which are very abundant on the Earth. Importantly, the g-C₃N₄ materials can be easily fabricated by thermal polymerization of abundant nitrogen-rich precursors such as melamine [7–16], dicyandiamide [17–22], cyanamide [23–25], urea [18,26,27], thiourea [28–30], ammonium thiocyanate [31–33], etc. Because the band gap of g-C₃N₄ is 2.7 eV, it can absorb visible light shorter than 450 nm effectively, implying broad prospects in solar energy conversion applications. Due to the aromatic C-N heterocycles, g-C₃N₄ is thermally stable up to 600 °C in air. Moreover, g-C₃N₄ is insoluble in acids, bases or organic solvents, exhibiting good chemical stability.

However, some bottlenecks in the photocatalytic activity of g-C₃N₄ still exist, such as fast photogenerated carrier recombination, limited active site, small specific surface area, low light absorption capacity, unsatisfactory crystallinity and unignorable surface

defects. How to promote the efficient migration and separation of photogenerated carriers, expand the spectral response range and increase the specific surface area of $g\text{-C}_3\text{N}_4$ is the core problem to achieve high energy conversion efficiency. In practice, the introduction of impurities into the $g\text{-C}_3\text{N}_4$ matrix through copolymerization and doping has become an effective strategy to change the electronic structure and band structure of $g\text{-C}_3\text{N}_4$. On the other hand, numerous research works have demonstrated that the physicochemical properties and photocatalytic efficiency of the polymer $g\text{-C}_3\text{N}_4$ can be significantly improved by optimizing synthesis techniques such as supramolecular and copolymerization techniques with identical structural and nano-structural designs, or by template-assisted methods to improve porosity and surface area [34–39]. Amongst various modification approaches, designing and constructing a more suitable band structure is the most important prerequisite to improve the charge separation efficiency, thereby enhancing the photocatalytic performance.

In this review, the synthesis parameters of $g\text{-C}_3\text{N}_4$ are discussed first, mainly including the types of $g\text{-C}_3\text{N}_4$ precursors, reaction temperature, reaction atmosphere and reaction duration. The influence of different synthesis parameters of $g\text{-C}_3\text{N}_4$ are compared and summarized in detail here. Then, the construction approaches of various nanostructures are reviewed, such as hard and soft template, supramolecular preorganization, template-free approaches, etc. It again manifests that the specific surface area and photocatalytic efficiency of $g\text{-C}_3\text{N}_4$ can be directly manipulated by means of different nanostructure design approaches. Furthermore, the characteristics of different exfoliation methods are summarized for stark comparisons. Liquid exfoliation of bulk $g\text{-C}_3\text{N}_4$ has gradually become the most popular exfoliation method. The overall framework of synthesis and properties of $g\text{-C}_3\text{N}_4$ for enhanced photocatalytic performance are illustrated in Figure 1. Finally, the problems of $g\text{-C}_3\text{N}_4$ materials in photocatalysis and the prospect of further development are proposed, which may be favorable to the design of more efficient and practical $g\text{-C}_3\text{N}_4$ or $g\text{-C}_3\text{N}_4$ -based photocatalyst.

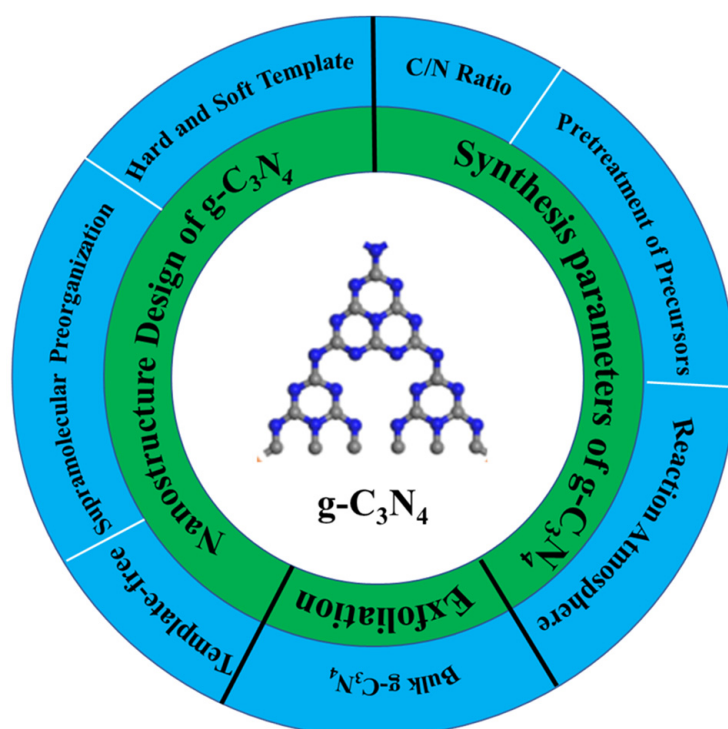


Figure 1. Overall framework of synthesis and properties of $g\text{-C}_3\text{N}_4$ for enhanced photocatalytic performance.

2. Influence of Synthesis Parameters

2.1. Precursors and Reaction Temperature

The first reported $g\text{-C}_3\text{N}_4$ as a heterogeneous catalysis was present in 2006 [40]. Subsequently, various precursors such as urea [41], thiourea [42], cyanamide [43,44] and dicyandiamide [45,46] have been employed to synthesize $g\text{-C}_3\text{N}_4$ by thermal treatment methods. In 2009, Wang et al. firstly used cyanamide as the precursor of $g\text{-C}_3\text{N}_4$ for producing hydrogen from water under visible-light irradiation in the presence of a sacrificial donor [47]. This pioneering work represents an important first step towards photosynthesis in general, where artificial conjugated polymer semiconductors can be used as energy transducers. In order to demonstrate the reaction intermediate compounds, characterization techniques such as thermogravimetric analysis (TGA) and X-ray diffraction (XRD) are used to characterize the reaction. Figure 2a displayed that the graphitic planes are constructed from tri-s-triazine units connected by planar amino groups. Figure 2b is the XRD pattern of the obtained $g\text{-C}_3\text{N}_4$ powder. From the ultraviolet-visible spectrum (Figure 2c), it can be seen that the band gap of $g\text{-C}_3\text{N}_4$ is 2.7 eV. The synthesis of $g\text{-C}_3\text{N}_4$ was a combination of polyaddition and polycondensation. At a reaction temperature of 203 and 234 °C, the cyanamide molecules can be condensed to dicyandiamide and melamine, respectively. The ammonia is then removed by condensation. When the temperature reaches 335 °C, large amounts of melamine products are detected. When further heating to 390 °C, the rearrangements of melamine will result in the formation of tri-s-triazine units. Finally, when heating to 520 °C, the polymeric $g\text{-C}_3\text{N}_4$ are synthesized via the further condensation of the unit. However, $g\text{-C}_3\text{N}_4$ will be unstable at above 600 °C. Furthermore, when the reaction degree is higher than 700 °C, $g\text{-C}_3\text{N}_4$ will decompose. Figure 2d shows the structural phase transition process from cyanamide to $g\text{-C}_3\text{N}_4$ at different temperatures. In addition to in-situ characterization experiments to verify the reaction process, it can also be demonstrated by relevant simulation calculations. The first-principles DFT calculations were performed using a plane wave basis set with a 550 eV energy cutoff [40]. The calculation results showed that the cohesion energy increased under the addition of multiple reaction pathways, which confirmed that melamine was produced upon heating the cyanamide, as shown in Figure 2e. In another work, Ang et al. demonstrated that when thiourea is used as the precursor and TiO_2 or SiO_2 are used as the inorganic substrate, the melon nanocomposites can be formed at a low temperature of 400 °C [48]. However, the degree of polymerization of $g\text{-C}_3\text{N}_4$ in the nanocomposites is low, so its photocatalytic performance is moderate. Following this, Zhang et al. reported a simple method of $g\text{-C}_3\text{N}_4$ synthesis from thiourea without the aid of any substrates [49]. It was found that the obtained $g\text{-C}_3\text{N}_4$ exhibited a good condensation likely due to the presence of sulfur species in thiourea, thus accelerating the degree of polymerization and condensation of thiourea at high temperatures. Having insights into the results of different reports, it can be found that different precursors have distinct characteristics and advantages. In order to obtain well-condensed $g\text{-C}_3\text{N}_4$ with high quality, the most crucial point is to select the best reaction temperature corresponding to the selected precursor.

In order to prove that $g\text{-C}_3\text{N}_4$ has been successfully prepared, a variety of analytical measurements can be used, such as X-ray photoelectron spectroscopy (XPS), XRD and Fourier transform infrared (FTIR) spectroscopy. The basic experimental procedures for the synthesis, characteristics of different precursors and characterization of $g\text{-C}_3\text{N}_4$ are described above. What effects other synthesis parameters have on $g\text{-C}_3\text{N}_4$ will be compared and discussed in detail in the following sections.

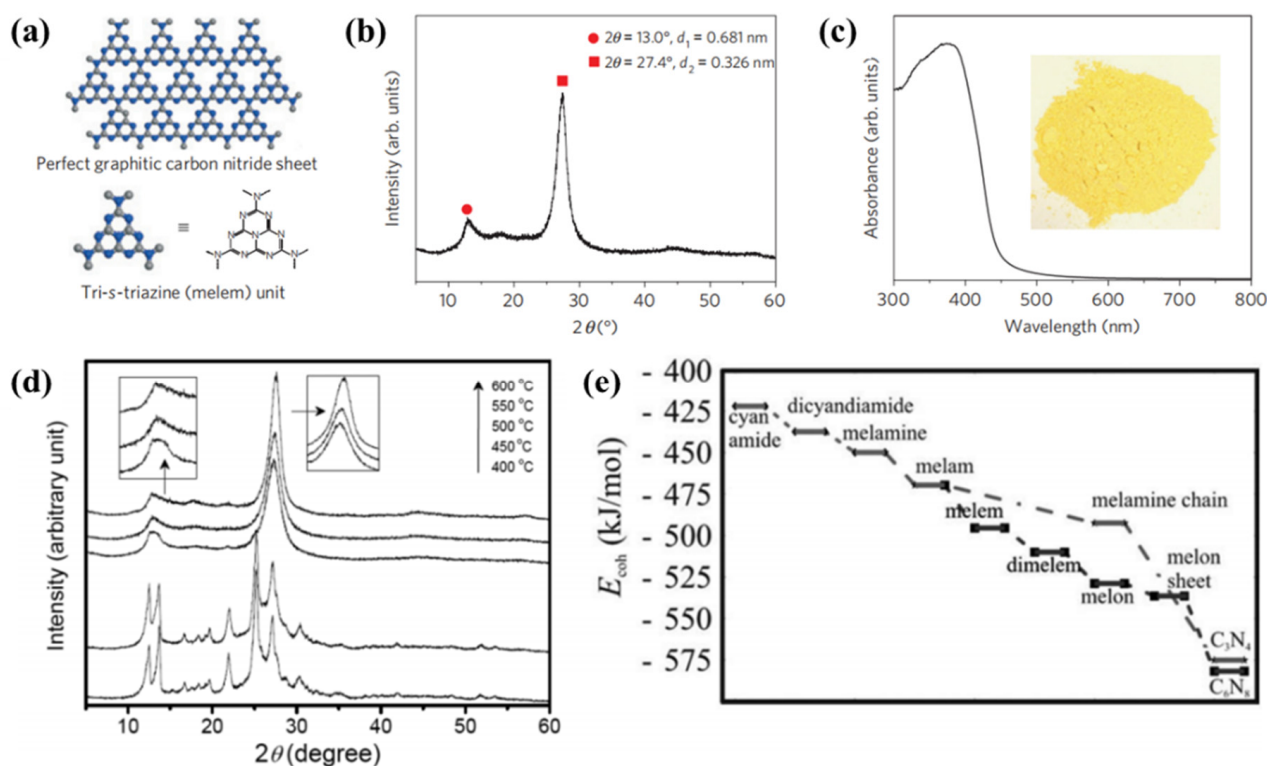


Figure 2. Crystal structure and optical properties of $g\text{-C}_3\text{N}_4$. (a) Schematic diagram of a perfect $g\text{-C}_3\text{N}_4$ sheet constructed from melem units. (b) Experimental XRD pattern of polymeric carbon nitride, revealing a graphitic structure with an interplanar stacking distance of the aromatic unit (0.326 nm). (c) Diffuse reflectance spectrum of the polymeric carbon nitride. Inset: Photograph of the photocatalyst. (d) XRD patterns of $g\text{-C}_3\text{N}_4$ treated at different temperatures. (e) Calculated energy diagram for the development of $g\text{-C}_3\text{N}_4$ using cyanamide precursor [47].

2.2. C/N Ratio

Generally, $g\text{-C}_3\text{N}_4$ exhibits a high physicochemical stability and ideal band structure, due to the high condensation degree and the presence of the heptazine ring structure. When the appropriate precursor and condensation method are selected, the C/N ratio in layered $g\text{-C}_3\text{N}_4$ is about 0.75. Many studies have confirmed that when the precursors and synthesis parameters of $g\text{-C}_3\text{N}_4$ are changed, the physicochemical properties of $g\text{-C}_3\text{N}_4$ will be significantly affected, such as band gap width, specific surface area, C/N ratio, etc., which will directly affect the photocatalytic efficiency and other applications' performance [50–54]. Yan et al. synthesized $g\text{-C}_3\text{N}_4$ by directly heating the low-cost melamine, and they change the C/N ratio by controlling different heating temperatures [55]. The research showed that when the heating temperatures increased from 500 to 580 °C, the ratio of C/N increased from 0.721 to 0.742. Meanwhile, the band gaps of $g\text{-C}_3\text{N}_4$ decreased from 2.8 to 2.75 eV. Apparently, increasing the heat temperature will decrease the photooxidation ability of $g\text{-C}_3\text{N}_4$. The C/N ratio, i.e., the degree of condensation, is inconsistent with the structural integrity. Therefore, in order to obtain a better photocatalytic efficiency, reasonable optimization measures must be taken to make the C/N ratio closer to the ideal ratio (0.75) [56]. Therefore, the presence of trace amino groups is actually conducive to improving the surface activity of $g\text{-C}_3\text{N}_4$, thus exhibiting better interaction with the reactant molecules [8,57,58]. However, due to incomplete concentration, the C/N ratio is lower than the ideal value (0.75), resulting in a large number of defects, inhibiting the rate of carrier transport and separation, and seriously reducing the photocatalytic efficiency. Therefore, in order to obtain a relatively high photocatalytic efficiency, the optimal C/N ratio is 0.75, which can usually reflect that $g\text{-C}_3\text{N}_4$ has a good concentration and stability.

2.3. Pretreatment of Precursors

It has been shown that modification and pretreatment of nitrogen-rich precursors before thermal annealing can effectively improve the physicochemical properties of g-C₃N₄. One of the effective pretreatment methods is by acid treatment. Yan et al. reported the synthesis of g-C₃N₄ by directly heating the sulfuric-acid-treated melamine precursor [59]. It is worth noting that the carbon nitride synthesized from sulfuric acid treated melamine (15.6 m²/g) shows relatively higher BET surface area than that of samples synthesized from untreated melamine (8.6 m²/g). The reason can be attributed to the effect of pretreatment of melamine with H₂SO₄ on its condensation process, during which sublimation of melamine is inhibited significantly. In addition to the pretreatment of melamine with H₂SO₄, HCl and HNO₃ also exhibited good pretreatment effects on melamine [60–63].

In addition to acid precursors, pretreatment methods of sulfur-mediated synthesis can also be used to regulate the structure and physicochemical properties of g-C₃N₄ [64]. The fundamental reason is that the presence of the sulfur group in the sulfur-containing thiourea provides an additional chemical pathway to regulate the degree of condensation and polymerization of g-C₃N₄ because it is easy to leave the -SH groups. Zhang et al. advanced this strategy by employing cheap and easily available elemental sulfur as the external sulfur species instead of sulfur-containing precursors for the sulfur-mediated synthesis of g-C₃N₄ photocatalysts [65]. In comparison with unmodified g-C₃N₄, the vibrations of g-C₃N₄-S_x are less intensive when increasing the amount of elemental sulfur (S₈), especially for the broad band at 2900–3300 cm⁻¹. Thus, S₈-mediated synthesis helps to advance the polymerization of melamine precursors, leaving fewer amino-containing groups as surface defects. In this report, the structure, electronic and optical properties of g-C₃N₄ have been effectively modified, and its physicochemical properties have also been significantly improved. Under visible light irradiation at 420 nm, the photocatalytic activity of water reduction and oxidation was enhanced.

2.4. Reaction Atmosphere

In addition to the types of precursors, reaction temperature and duration, the physicochemical properties and structure of g-C₃N₄ are also strongly influenced by the reaction atmosphere, because the reaction atmosphere can induce a variety of defects and carbon and nitrogen vacancies. In fact, defects are essential for catalytic reactions because they can act as active sites for reactant molecules and change the band structure by introducing additional energy levels in the forbidden band, thus extending the spectral absorption range [66–69]. By controlling the polycondensation temperature of a dicyandiamide precursor in the preparation of g-C₃N₄, Niu et al. introduced nitrogen vacancies in the framework of g-C₃N₄ [70]. The excess electrons caused by nitrogen loss in g-C₃N₄ lead to a large number of C³⁺ states associated with nitrogen vacancies in the band gap, thus reducing the intrinsic band gap from 2.74 eV to 2.66 eV. Steady and time-resolved fluorescence emission spectra show that, due to the existence of abundant nitrogen vacancies, the intrinsic radiative recombination of electrons and holes in g-C₃N₄ is greatly restrained, and the population of short-lived and long-lived charge carriers is decreased and increased, respectively. In another study, Niu et al. produced a novel visible light photocatalyst R-melon by heating the melon in a hydrogen atmosphere [71]. Compared to the pristine melon with a bandgap of 2.78 eV, the resultant R-melon with a bandgap of 2.03 eV has a widened visible light absorption range and suppressed radiative recombination of photo-excited charge carriers due to homogeneous self-modification with nitrogen vacancies. Table 1 shows the summary of the specific surface areas and band gaps of g-C₃N₄ photocatalysts developed from various precursors and different reaction parameters. The results demonstrated that the band structure, electronic properties and specific surface area of g-C₃N₄ can be changed by adjusting the reaction parameters and precursors, so as to improve its photocatalytic performance.

Table 1. Precursors and Reaction Parameters Employed in the g-C₃N₄ Synthesis.

Precursors	Synthesis Parameters	Surface Area (m ² g ⁻¹)	Band Gap Energy (eV)	Ref.
Cyanamide	550 °C, 4 h, air	10	2.7	[47]
Dicyandiamide	550 °C, 3 h, air	12.3	2.66	[56]
Dicyandiamide	600 °C, 4 h, air	12.8	2.75	[72]
Dicyandiamide	550 °C, 4 h, H ₂	20.91	2.0	[73]
Melamine	500 °C, 2 h, air	7.1	2.83	[74]
Melamine	520 °C, 2 h, N ₂	17.4	2.74	[75]
H ₂ SO ₄ -treated melamine	600 °C, 4 h, Ar	15.6	2.69	[59]
HCl-treated melamine	550 °C, 4 h, air	26.2	2.73	[61]
Thiourea	550 °C, 3 h, air	11.3	2.6	[56]
Urea	450 °C, 2 h, air	135.6	2.76	[76]

3. Morphology and Structure Design of g-C₃N₄

3.1. Hard and Soft Template Approach

Apart from regulating the synthesis parameters, introducing nano-templates and nano-casting with different morphology and ordered porosity on the basis of bulk g-C₃N₄ is another promising method to change the morphology and structural characteristics of g-C₃N₄ structure and the interlayer interaction. As a matter of fact, researchers have effectively designed controllable nanostructures for g-C₃N₄ through hard template or soft template methods, such as porous g-C₃N₄, one-dimensional nanostructures, hollow g-C₃N₄ nanospheres, etc [11,77–85]. It has been proven that the porosity, structure, morphology, surface area and size can be easily controlled by adjusting the appropriate template. Moreover, the larger surface area and more active sites are generally more favorable for photocatalytic applications of g-C₃N₄.

The hard template method is almost identical to the traditional casting process and is one of the most common techniques for developing nanostructured g-C₃N₄ materials. In this way, the various structures and geometries of g-C₃N₄ can be designed using hard templates as needed, and their length scales are usually around nanometers and microns. The most typical structure-oriented agent is a silica template with a controllable nanostructure. The early study on the mesoporous g-C₃N₄ synthesized using cyanamide as a precursor and silica nanoparticles with a size of 12 nm as a template was reported by Goettmann et al. [40]. The results show that the silica nanoparticles can be uniformly dispersed in the cyanamide monomer, which is due to the appropriate surface interaction between the silica surface and the amine and aromatic nitrogen groups. After heating treatment and cyanamide condensation, the g-C₃N₄/silica hybrid is formed, and well-dispersed silica nanoparticles are preserved in the g-C₃N₄ matrix. Ammonium hydrogen fluoride (NH₄HF₂) solution can be used to remove the silicon template. The average diameter is 12 nm, and the surface area in the range of 86 to 439 m² g⁻¹ can be regulated by adjusting the mass ratios of silica/cyanamide from 0 to 1.6. In another work carried out by Yuki Fukasawa et al., uniform-sized silica nanospheres (SNSs) assembled into close-packed structures were used as a primary template for ordered porous g-C₃N₄, which was subsequently used as a hard template to generate regularly arranged Ta₃N₅ nanoparticles of well-controlled size [86]. The cyanamide is infiltrated and polymerized in the narrow void of SNSs to form porous g-C₃N₄, and then the SNSs is removed by HF treatment, as shown in Figure 3a. Therefore, the resulting g-C₃N₄ has an anti-opal structure, and the size of the spherical hole indicates the size of the SNSs used, as shown in the SEM images of Figure 3b–e. In this study, the pore size of g-C₃N₄ was between 50 and 80 nm. In spite of the silica hard template, Chen et al. reported the synthesis of porous g-C₃N₄ by using multi-walled carbon nanotube (CNT) as a novel hard template [87]. Unlike other hard templates, CNT can be easily removed and recovered by ultrasonic methods, resulting in a relatively simple preparation of porous g-C₃N₄.

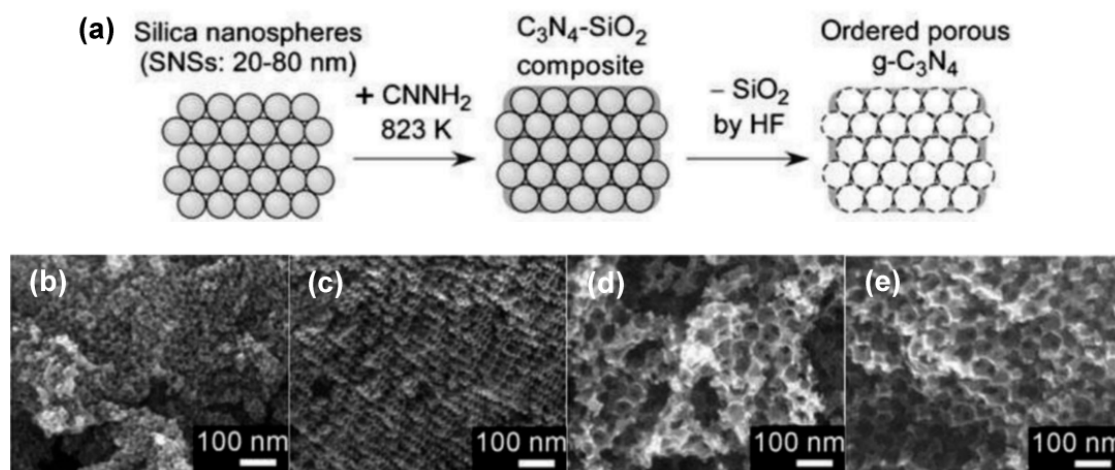


Figure 3. (a) Synthesis procedure of ordered porous $g\text{-C}_3\text{N}_4$. Field emission SEM (FESEM) images of porous $g\text{-C}_3\text{N}_4$ prepared using silica spheres with various diameters: (b) 20, (c) 30, (d) 50, and (e) 80 nm [86].

It can be seen that during the synthesis of $g\text{-C}_3\text{N}_4$ through hard templates, extremely dangerous, toxic and expensive fluorine-containing etchers (such as HF and NH_4HF_2) are used to remove the sacrificial templates. This greatly limits the practical application of the method in large-scale industrial processes. Therefore, apart from the hard template synthesis method of $g\text{-C}_3\text{N}_4$, the relatively “environmentally friendly” soft template process can not only change the morphology and structure of $g\text{-C}_3\text{N}_4$ through the selection of multiple soft templates, but also simplify the synthesis route of $g\text{-C}_3\text{N}_4$ [88,89]. Different from the hard template method, in the soft template method, the nano-structure $g\text{-C}_3\text{N}_4$ is synthesized by soft structure guiding agents such as ionic liquid, amphiphilic block polymer and surfactant, so as to rationally design $g\text{-C}_3\text{N}_4$ with a highly porous nanostructure [90]. For instance, bimodal mesoporous $g\text{-C}_3\text{N}_4$ is synthesized using Triton X-100 as a soft-template and melamine and glutaraldehyde as precursors through polymerization and carbonization [91]. The results show that the mesopore sizes in the $g\text{-C}_3\text{N}_4$ are centered at 3.8 nm and 10–40 nm. The former was attributed to the removal of the Triton X-100, while the latter was ascribed to the aggregates of plate-like $g\text{-C}_3\text{N}_4$. In another study reported by Wang et al., a variety of soft-templates (e.g., Triton X-100, P123, F127, Brij30, Brij58, and Brij76) as well as some ionic surfactants are tested as structure-directing agents for the synthesis of mesoporous $g\text{-C}_3\text{N}_4$ [90]. Most as-prepared $g\text{-C}_3\text{N}_4$ materials possess a high surface area. Moreover, this work points out two problems. The first was that only a few selected soft templates (Triton X-100 and ionic liquids) led to the presence of mesoporous $g\text{-C}_3\text{N}_4$ structures with high surface areas. Due to the premature decomposition of the template material, the pores of $g\text{-C}_3\text{N}_4$ are easily resealed. The second problem is that the obtained $g\text{-C}_3\text{N}_4$ contains a large amount of carbon elements from the template polymer, which significantly changes the morphology and structure of $g\text{-C}_3\text{N}_4$, thereby reducing its photocatalytic activity.

Overall, it is not difficult to find that the synthesis of $g\text{-C}_3\text{N}_4$ with various nanostructures assisted by hard and soft templates is a facile and efficient approach. Nowadays, researchers are still developing a variety of new templates to achieve more interesting $g\text{-C}_3\text{N}_4$ nanostructures with high photocatalytic efficiency.

3.2. Supramolecular Preorganization Approach

In contrast to the previously discussed hard and soft template synthesis approaches, molecular self-assembly is a self-templating approach (namely supramolecular preorganization approach) in which molecules spontaneously form a stable $g\text{-C}_3\text{N}_4$ structure from non-covalent bonds under equilibrium conditions in the absence of an external template [80,92–94]. Recently, supramolecular preassembly of triazine molecules has become an

interesting method to regulate the structural, textural, optical, and electronic features of $g\text{-C}_3\text{N}_4$, thus affecting its photocatalytic activity [95–98]. For example, nanostructured $g\text{-C}_3\text{N}_4$ materials can be developed by supramolecular preorganization of melamine precursors to triazine derivatives to form hydrogen bond molecular assemblies, i.e., melamine–cyanuric acid, melamine–trithiocyanuric acid mixtures or their derivatives [99–101]. Jun et al. first synthesized $g\text{-C}_3\text{N}_4$ by molecular cooperative assembly between triazine molecules [102]. Flower-like, layered spherical aggregates of melamine cyanuric acid complex (MCA) are formed by precipitation from equimolecular mixtures in dimethyl sulfoxide (DMSO). The oxygen-containing intermolecular structure connected by hydrogen bonding and stacked in graphitic fashion facilitates the condensation process and enables structural perfection. The obtained material synthesized by this supramolecular preorganization approach has stronger spectral absorption (an increased band gap of 0.16 eV), and the photogenerated carrier lifetime is extended nearly twice as long as that of bulk $g\text{-C}_3\text{N}_4$.

It can be seen that the combination of two or more monomers in different solvents can form supramolecular complexes. These supramolecular complexes are usually linked by hydrogen bonds. Therefore, it is expected that the addition of new monomers to hydrogen-bonded supramolecular complexes as “terminators” will be an attractive technique to further adjust the morphology, photophysical properties, and electronic band structure of $g\text{-C}_3\text{N}_4$.

3.3. Template-Free Approach

Compared with the hard and soft template synthesis approaches, the template-free approach has unique advantages, such as no need for various high-cost and dangerous templates containing fluorine, and no residue of any template components. Indeed, many studies have proven that $g\text{-C}_3\text{N}_4$ nanostructure designs with a variety of morphologies and desired sizes, such as nanorods, quantum dots, microspheres, nanofibers, etc., can also be achieved using a template-free approach. Bai et al. reported that the transformation of $g\text{-C}_3\text{N}_4$ from nanoplates to nanorods was realized by a simple reflux method [103]. Various aspect ratios were achieved by changing the reflux duration and solvent ratio without the assistance of any templates. As per the TEM images shown in Figure 4a–d, most irregular nanoplates are observed in the untreated $g\text{-C}_3\text{N}_4$ sample, while the refluxed $g\text{-C}_3\text{N}_4$ sample mainly contains nanorods. The length of $g\text{-C}_3\text{N}_4$ nanorods is 0.5–3 μm . The growth mechanism and process can be summarized as follows (Figure 4e): under ultrasonic action, CH_3OH can strip $g\text{-C}_3\text{N}_4$ bulks into nanosheets. The reflux process can remove surface defects and transform them into nanorods. After reflux treatment, the $g\text{-C}_3\text{N}_4$ nanosheets showed the metastable state. With the increase of time, the layered structure of $g\text{-C}_3\text{N}_4$ will curl and finally grow into nanorods. Finally, the shorter $g\text{-C}_3\text{N}_4$ nanorods are redissolved into the solution, while the longer nanorods will continue to grow during reflux treatment. The increase in visible light degradation activity of methylene blue can be induced for the increase of active lattice face and elimination of surface defects.

Additionally, Wang et al. described a facile and generally feasible method to synthesize nanotube-type $g\text{-C}_3\text{N}_4$ by directly heating melamine packed in an appropriate compact degree without templates [104]. A certain amount of melamine was placed into a semi-closed alumina crucible followed by consecutively shaking the crucible using a vibrator at a fast rate to achieve a moderately compact packing degree. This process is very crucial for the synthesis of nanotube-type $g\text{-C}_3\text{N}_4$. TEM images show that the wall thickness of the nanotubes in the bulk phase is about 15 ± 2 nm, while the inner diameter is about 18 ± 2 nm. In this report, the formation process and mechanism of nanotubes have been studied in detail. During the pyrolysis process, melamine releases NH_3 gas, which passes through the stacked melamine layers to form rolled $g\text{-C}_3\text{N}_4$ nanosheets. Due to the need to reduce the surface free energy, the nanosheets eventually bend into the form of nanotubes. It is worth pointing out that when the melamine layer is loosely stacked, $g\text{-C}_3\text{N}_4$ cannot form a nanotube structure, which indicates that obtaining the appropriate packing degree of $g\text{-C}_3\text{N}_4$ is crucial for the formation of the nanotube structure.

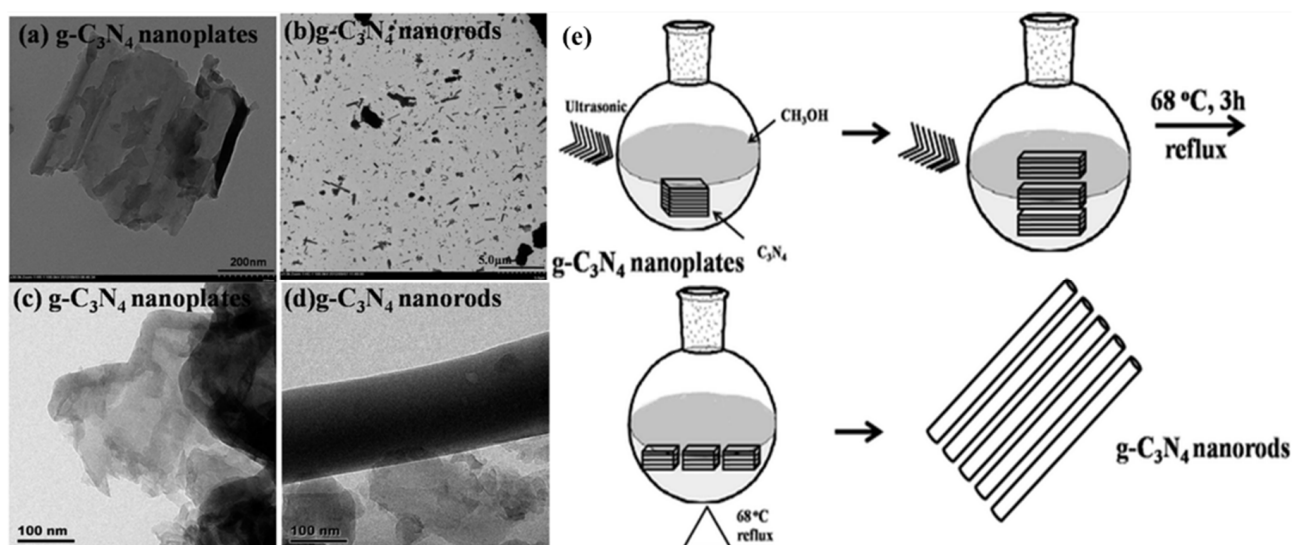


Figure 4. TEM images of $g\text{-C}_3\text{N}_4$ nanoplates (a,c) and nanorods (b,d). (e) Schematic illustration of the formation processes of $g\text{-C}_3\text{N}_4$ nanorods from $g\text{-C}_3\text{N}_4$ nanoplates [103].

4. Exfoliation of Bulk $g\text{-C}_3\text{N}_4$

Although the specific surface area of the monolayer $g\text{-C}_3\text{N}_4$ is theoretically large, the specific surface area of the block is very low indeed, usually less than $10\text{ m}^2\text{ g}^{-1}$, due to the stacking of $g\text{-C}_3\text{N}_4$ layers [105]. Therefore, delaminating $g\text{-C}_3\text{N}_4$ into several layers is a promising way to improve photocatalytic performance and produce more interesting surface, optical and electronic properties [106–109]. There are many methods of exfoliating $g\text{-C}_3\text{N}_4$, such as ultrasonication-assisted liquid exfoliation, the liquid ammonia-assisted lithiation and the post-thermal oxidation etching route [17,108–115]. Similar to most two-dimensional materials, there is a weak van der Waals force between the layers of $g\text{-C}_3\text{N}_4$. Thus, the van der Waals force can be effectively overcome and the separation between layers can be achieved by means of energy assistance such as ultrasound in an appropriate solvent.

Liquid exfoliation is simple and convenient, and has gradually become the most commonly used exfoliation method by most researchers. Yang et al. demonstrated the synthesis of free-standing $g\text{-C}_3\text{N}_4$ nanosheets by liquid phase exfoliation [110]. The method uses $g\text{-C}_3\text{N}_4$ powder as a starting material and various organic solvents (such as isopropanol (IPA), N-methyl-pyrrolidone (NMP), acetone, and ethanol) as dispersing media. As shown in Figure 5a,b, many nanosheets with laminar morphology like silk veil can be observed, which is in stark contrast from that of bulk $g\text{-C}_3\text{N}_4$. The photographs in Figure 5e clearly demonstrated that NMP is a promising dispersing solvent among various dispersing solvents. It can stably disperse individual nanosheets; however, the disadvantage is that the boiling point of NMP is relatively high, which is difficult to remove. The agglomeration phenomenon of $g\text{-C}_3\text{N}_4$ layer can be observed in NMP. In comparison, low-boiling-point IPA is the best medium for preparing $g\text{-C}_3\text{N}_4$. The obtained $g\text{-C}_3\text{N}_4$ in IPA exhibited a surface area of up to $384\text{ m}^2\text{ g}^{-1}$ and a thickness of about 2 nm, as shown in Figure 5c,d. Moreover, the stability of IPA is superior, and there is no precipitation phenomenon after 4 months of storage (Figure 5f).

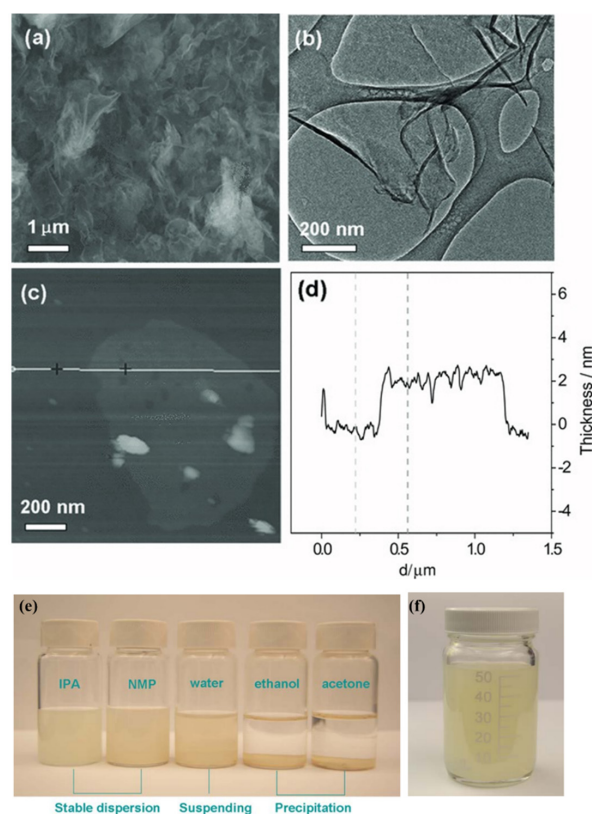


Figure 5. Typical FESEM (a) and TEM (b) images unveiling the flexible $g\text{-C}_3\text{N}_4$ nanosheets with the size from 500 nm to several micrometers. Representative AFM image (c) and corresponding thickness analysis (d) taken around the white line (c) revealing a uniform thickness of about 2 nm for $g\text{-C}_3\text{N}_4$ nanosheets. (e) Photographs of the $g\text{-C}_3\text{N}_4$ nanosheet dispersions in IPA, NMP, water, ethanol and acetone, respectively, after 2 days storage under ambient conditions, and (f) in IPA solvent after 4 months storage [110].

5. Doping of $g\text{-C}_3\text{N}_4$

It is well-known that $g\text{-C}_3\text{N}_4$ is a metal-free n-type semiconductor. Due to the high ionization energy and high electronegativity of metal-free semiconductors, it is easy for them to form covalent bonds with other compounds by obtaining electrons during the reaction. In order to maintain this unique advantage of metal-free semiconductors, researchers have implemented a series of non-metal doping $g\text{-C}_3\text{N}_4$, including oxygen, phosphorus, sulfur, carbon, halogen, nitrogen and boron [116–121]. For instance, O-doping is a facile method to improve the photocatalytic ability of $g\text{-C}_3\text{N}_4$. Zeng et al. synthesized one-dimensional porous architectural $g\text{-C}_3\text{N}_4$ nanorods by direct calcination of hydrous melamine nanofibers precipitated from an aqueous solution of melamine [122]. The porous structure increases the specific surface area, enhances the light absorption capacity and improves the catalytic reaction rate. At the same time, doping oxygen atoms into the $g\text{-C}_3\text{N}_4$ matrix breaks the symmetry of the pristine structure, making more efficient separation of electron/hole pairs. In general, non-metallic doping usually changes the surface morphology and structure of $g\text{-C}_3\text{N}_4$, thereby affecting the light absorption efficiency and regulating the catalytic efficiency.

Different from non-metal doping, metal-doped $g\text{-C}_3\text{N}_4$ has the advantages of reducing band gap to enhance visible light absorption and to improve catalytic performance. Commonly used doped metals include alkali metals (Li, Na, K) and transition metals (Fe, Cu, and W) [123–127]. For example, Xiong et al. reported that the doping of alkali metals (K, Na) in the $g\text{-C}_3\text{N}_4$ framework significantly increases the transfer and separation rates of photogenerated carriers and induces more efficient redox catalytic reactions [128]. DFT calculation results showed that K or Na doping can reduce the band gap energy of

$g\text{-C}_3\text{N}_4$. Generally, the introduction of metal ions can form new energy levels, increase the specific surface area, and sometimes resist the recombination of charge carriers produced by photons. The catalytic efficiency of noble metal doping is usually higher, but the photodegradation efficiency of some ordinary transition-metal-doped $g\text{-C}_3\text{N}_4$ for some pollutants can be comparable to that of noble-metal-doped $g\text{-C}_3\text{N}_4$ when the appropriate doping amount and mode are selected.

6. Applications of $g\text{-C}_3\text{N}_4$

Due to its moderate energy gap, excellent electronic properties, rich functional groups and surface defects, $g\text{-C}_3\text{N}_4$ can be widely used in environmental treatment and pollutant degradation, including water splitting, hydrogen generation, CO_2 conversion and organic pollutants degradation [129–132].

As reported, the pristine $g\text{-C}_3\text{N}_4$ has limitations such as small specific surface area and fast charge recombination rate, which leads to a low water splitting ability of $g\text{-C}_3\text{N}_4$. To solve this problem, Chen et al. improved the water splitting capacity via adjusting the dimension of $g\text{-C}_3\text{N}_4$ [133]. As shown in Figure 6a,b, they demonstrated that the evolution rates of H_2 and O_2 of three-dimensional porous $g\text{-C}_3\text{N}_4$ in visible light are significantly higher than those of the pristine $g\text{-C}_3\text{N}_4$, reaching 101.4 and $49.1 \mu\text{mol g}^{-1} \text{h}^{-1}$, respectively. Fu et al. reported oxygen-doped $g\text{-C}_3\text{N}_4$ [134]. As exhibited in Figure 6c-d, the O-doped $g\text{-C}_3\text{N}_4$ has a narrower band gap and greater CO_2 affinity, which significantly improves the photogenerated carrier separation efficiency and CO_2 conversion ability. In addition, a lot of efforts have been made to enhance its photocatalytic activity to improve its pollutant degradation ability. As shown in Figure 6e-f, Dou et al. reported that mesoporous $g\text{-C}_3\text{N}_4$ has a strong ability to remove antibiotics under visible light [135], which is mainly due to the porous structure that improved the utilization of light.

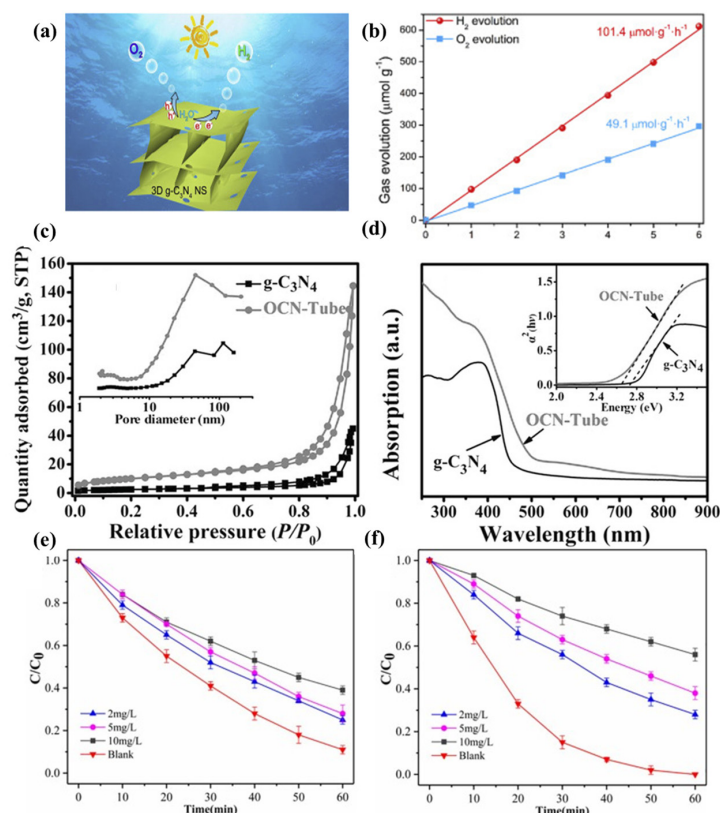


Figure 6. (a) Water splitting for H_2 and O_2 Evolution. (b) Time–dependent overall water splitting over 3D $g\text{-C}_3\text{N}_4$ [133]. (c) N_2 adsorption–desorption isotherms and corresponding pore size distribution curves. (d) UV–vis diffuse reflectance spectra [134]. The effects of humic acid on (e) amoxicillin and (f) cefotaxime photodegradation by mesoporous carbon nitride (initial pH = 7) [135].

7. Conclusions and Prospects

In summary, due to the merits of low cost, high stability and visible light response, g-C₃N₄ is one of the most promising photocatalytic materials to replace TiO₂. This review mainly introduces the synthesis of g-C₃N₄, the improvement of the g-C₃N₄ crystal structure, the light absorption enhancement, structure design optimization, as well as the improvement of electronic properties and optimization of energy band, so as to promote the photocatalytic application of g-C₃N₄. As summarized above, the appropriate reaction temperature and duration of the condensation process are beneficial to improve the crystallinity of g-C₃N₄. Various desirable nanostructures of g-C₃N₄ can be constructed via hard and soft template approaches, supramolecular preorganization approach, and template-free approach. Liquid exfoliation of bulk g-C₃N₄ has becoming the most facile and promising method to improve the surface area of g-C₃N₄.

Therefore, in order to synthesize the ideal g-C₃N₄ with high photocatalytic efficiency, it is necessary to pay attention to the following crucial elements: (i) Controlling the corresponding reaction temperature and reaction time according to the selected precursor material; (ii) Controlling the C/N ratio close to 0.75 and the band gap to 2.7 eV; (iii) Extending the specific surface area by selecting suitable nanostructure design approaches.

It can be assumed that in the future, g-C₃N₄, a booming photocatalytic hot spot material, will face unlimited opportunities and challenges. Although g-C₃N₄ can be easily synthesized by thermal polymerization of nitrogen-rich precursors, its photocatalytic efficiency is not high due to its small specific surface area, limited surface reaction sites, and insufficient utilization of broad-spectrum sunlight. Here, some pivotal issues are elaborated in the following:

- (i) So far, the use of visible and near-infrared light is far from sufficient. On the one hand, it depends on the synthesis and structural design of the g-C₃N₄ material; on the other hand, a third or more component with a suitable band structure can also be cleverly added to design the interface electronic structure and expand the optical absorption region.
- (ii) Due to the limited surface area of g-C₃N₄ and the inevitable defects on the surface, the smooth transfer of photogenerated carriers is hindered. Therefore, the synthesis approached needs to be further developed. In order to optimize photocatalytic performance, some environmentally friendly, simple and efficient synthesis routes are urgently required.
- (iii) The integration of photocatalytic applications in many fields into one photocatalytic system is a widely used catalytic process. This requires the hybridization of multifunctional materials with reasonable energy structure. How to optimize the energy band structure and surface topography of g-C₃N₄ reasonably to improve the compatibility of energy conversion and environmental protection is very promising.
- (iv) More theoretical studies about g-C₃N₄ need to be combined with practical catalytic applications. It is certain that in-depth fundamental theory based on physical chemistry research, in collaboration with laboratory findings, will positively promote the advances in materials science and technology.

Author Contributions: Conceptualization, S.Z. and D.Z.; investigation, H.L.; writing—original draft preparation, J.P. and D.Y. All authors have read and agreed to the published version of the manuscript.

Funding: This research received no external funding.

Conflicts of Interest: The authors declare no conflict of interest.

References

1. Wang, S.; Sun, L.; Iqbal, S. Green financing role on renewable energy dependence and energy transition in E7 economies. *Renew. Energy* **2022**, *200*, 1561–1572. [[CrossRef](#)]

2. Xu, M.-L.; Lu, M.; Qin, G.-Y.; Wu, X.-M.; Yu, T.; Zhang, L.-N.; Li, K.; Cheng, X.; Lan, Y.-Q. Piezo-Photocatalytic Synergy in BiFeO₃@COF Z-Scheme Heterostructures for High-Efficiency Overall Water Splitting. *Angew. Chem.-Int. Ed.* **2022**, *61*, e202210700. [[CrossRef](#)] [[PubMed](#)]
3. Miao, Z.; Wang, Q.; Zhang, Y.; Meng, L.; Wang, X. In situ construction of S-scheme AgBr/BiOBr heterojunction with surface oxygen vacancy for boosting photocatalytic CO₂ reduction with H₂O. *Appl. Catal. B-Environ.* **2022**, *301*, 120802. [[CrossRef](#)]
4. Peng, X.; Wu, J.; Zhao, Z.; Wang, X.; Dai, H.; Wei, Y.; Xu, G.; Hu, F. Activation of peroxymonosulfate by single atom Co-N-C catalysts for high-efficient removal of chloroquine phosphate via non-radical pathways: Electron-transfer mechanism. *Chem. Eng. J.* **2022**, *429*, 132245. [[CrossRef](#)]
5. Bai, J.; Shen, R.; Jiang, Z.; Zhang, P.; Li, Y.; Li, X. Integration of 2D layered CdS/WO₃ S-scheme heterojunctions and metallic Ti₃C₂ MXene-based Ohmic junctions for effective photocatalytic H₂ generation. *Chin. J. Catal.* **2022**, *43*, 359–369. [[CrossRef](#)]
6. Chen, T.; Yu, K.; Dong, C.; Yuan, X.; Gong, X.; Lian, J.; Cao, X.; Li, M.; Zhou, L.; Hu, B.; et al. Advanced photocatalysts for uranium extraction: Elaborate design and future perspectives. *Coord. Chem. Rev.* **2022**, *467*, 214615. [[CrossRef](#)]
7. Guo, S.; Deng, Z.; Li, M.; Jiang, B.; Tian, C.; Pan, Q.; Fu, H. Phosphorus-Doped Carbon Nitride Tubes with a Layered Micro-nanostructure for Enhanced Visible-Light Photocatalytic Hydrogen Evolution. *Angew. Chem.-Int. Ed.* **2016**, *55*, 1830–1834. [[CrossRef](#)]
8. Guo, S.; Tang, Y.; Xie, Y.; Tian, C.; Feng, Q.; Zhou, W.; Jiang, B. P-doped tubular g-C₃N₄ with surface carbon defects: Universal synthesis and enhanced visible-light photocatalytic hydrogen production. *Appl. Catal. B-Environ.* **2017**, *218*, 664–671. [[CrossRef](#)]
9. Liu, H.; Chen, D.; Wang, Z.; Jing, H.; Zhang, R. Microwave-assisted molten-salt rapid synthesis of isotype triazine-/heptazine based g-C₃N₄ heterojunctions with highly enhanced photocatalytic hydrogen evolution performance. *Appl. Catal. B-Environ.* **2017**, *203*, 300–313. [[CrossRef](#)]
10. Mo, Z.; Xu, H.; Chen, Z.; She, X.; Song, Y.; Wu, J.; Yan, P.; Xu, L.; Leia, Y.; Yuan, S.; et al. Self-assembled synthesis of defect-engineered graphitic carbon nitride nanotubes for efficient conversion of solar energy. *Appl. Catal. B-Environ.* **2018**, *225*, 154–161. [[CrossRef](#)]
11. Zhang, J.-W.; Gong, S.; Mahmood, N.; Pan, L.; Zhang, X.; Zou, J.-J. Oxygen-doped nanoporous carbon nitride via water-based homogeneous supramolecular assembly for photocatalytic hydrogen evolution. *Appl. Catal. B-Environ.* **2018**, *221*, 9–16. [[CrossRef](#)]
12. Zhu, B.; Xia, P.; Ho, W.; Yu, J. Isoelectric point and adsorption activity of porous g-C₃N₄. *Appl. Surf. Sci.* **2015**, *344*, 188–195. [[CrossRef](#)]
13. Huang, H.; Xiao, K.; Tian, N.; Dong, F.; Zhang, T.; Du, X.; Zhang, Y. Template-free precursor-surface-etching route to porous, thin g-C₃N₄ nanosheets for enhancing photocatalytic reduction and oxidation activity. *J. Mater. Chem. A* **2017**, *5*, 17452–17463. [[CrossRef](#)]
14. Tian, N.; Zhang, Y.; Li, X.; Xiao, K.; Du, X.; Dong, F.; Waterhouse, G.I.N.; Zhang, T.; Huang, H. Precursor-reforming protocol to 3D mesoporous g-C₃N₄ established by ultrathin self-doped nanosheets for superior hydrogen evolution. *Nano Energy* **2017**, *38*, 72–81. [[CrossRef](#)]
15. Wang, X.; Zhou, C.; Shi, R.; Liu, Q.; Waterhouse, G.I.N.; Wu, L.; Tung, C.-H.; Zhang, T. Supramolecular precursor strategy for the synthesis of holey graphitic carbon nitride nanotubes with enhanced photocatalytic hydrogen evolution performance. *Nano Res.* **2019**, *12*, 2385–2389. [[CrossRef](#)]
16. Zhou, C.; Shi, R.; Shang, L.; Wu, L.-Z.; Tung, C.-H.; Zhang, T. Template-free large-scale synthesis of g-C₃N₄ microtubes for enhanced visible light-driven photocatalytic H₂ production. *Nano Res.* **2018**, *11*, 3462–3468. [[CrossRef](#)]
17. Han, Q.; Wang, B.; Gao, J.; Cheng, Z.; Zhao, Y.; Zhang, Z.; Qu, L. Atomically Thin Mesoporous Nanomesh of Graphitic C₃N₄ for High-Efficiency Photocatalytic Hydrogen Evolution. *Acs Nano* **2016**, *10*, 2745–2751. [[CrossRef](#)]
18. Yang, P.; Ou, H.; Fang, Y.; Wang, X. A Facile Steam Reforming Strategy to Delaminate Layered Carbon Nitride Semiconductors for Photoredox Catalysis. *Angew. Chem.-Int. Ed.* **2017**, *56*, 3992–3996. [[CrossRef](#)]
19. Lan, Z.-A.; Zhang, G.; Wang, X. A facile synthesis of Br-modified g-C₃N₄ semiconductors for photoredox water splitting. *Appl. Catal. B-Environ.* **2016**, *192*, 116–125. [[CrossRef](#)]
20. Zhang, M.; Bai, X.; Liu, D.; Wang, J.; Zhu, Y. Enhanced catalytic activity of potassium-doped graphitic carbon nitride induced by lower valence position. *Appl. Catal. B-Environ.* **2015**, *164*, 77–81. [[CrossRef](#)]
21. Hu, S.; Ma, L.; You, J.; Li, F.; Fan, Z.; Lu, G.; Liu, D.; Gui, J. Enhanced visible light photocatalytic performance of g-C₃N₄ photocatalysts co-doped with iron and phosphorus. *Appl. Surf. Sci.* **2014**, *311*, 164–171. [[CrossRef](#)]
22. Hu, S.; Li, F.; Fan, Z.; Wang, F.; Zhao, Y.; Lv, Z. Band gap-tunable potassium doped graphitic carbon nitride with enhanced mineralization ability. *Dalton Trans.* **2015**, *44*, 1084–1092. [[CrossRef](#)] [[PubMed](#)]
23. Lan, H.; Li, L.; An, X.; Liu, F.; Chen, C.; Liu, H.; Qu, J. Microstructure of carbon nitride affecting synergetic photocatalytic activity: Hydrogen bonds vs. structural defects. *Appl. Catal. B-Environ.* **2017**, *204*, 49–57. [[CrossRef](#)]
24. Shen, Y.; Guo, X.; Bo, X.; Wang, Y.; Guo, X.; Xie, M.; Guo, X. Effect of template-induced surface species on electronic structure and photocatalytic activity of g-C₃N₄. *Appl. Surf. Sci.* **2017**, *396*, 933–938. [[CrossRef](#)]
25. Perez-Molina, A.; Pastrana-Martinez, L.M.; Morales-Torres, S.; Maldonado-Hodar, F.J. Photodegradation of cytostatic drugs by g-C₃N₄: Synthesis, properties and performance fitted by selecting the appropriate precursor. *Catal. Today* **2023**, *418*, 114068. [[CrossRef](#)]

26. Gao, Y.; Zhu, Y.; Lyu, L.; Zeng, Q.; Xing, X.; Hu, C. Electronic Structure Modulation of Graphitic Carbon Nitride by Oxygen Doping for Enhanced Catalytic Degradation of Organic Pollutants through Peroxymonosulfate Activation. *Environ. Sci. Technol.* **2018**, *52*, 14371–14380. [[CrossRef](#)] [[PubMed](#)]
27. Fang, J.; Fan, H.; Li, M.; Long, C. Nitrogen self-doped graphitic carbon nitride as efficient visible light photocatalyst for hydrogen evolution. *J. Mater. Chem. A* **2015**, *3*, 13819–13826. [[CrossRef](#)]
28. Yu, H.; Shi, R.; Zhao, Y.; Bian, T.; Zhao, Y.; Zhou, C.; Waterhouse, G.I.N.; Wu, L.-Z.; Tung, C.-H.; Zhang, T. Alkali-Assisted Synthesis of Nitrogen Deficient Graphitic Carbon Nitride with Tunable Band Structures for Efficient Visible-Light-Driven Hydrogen Evolution. *Adv. Mater.* **2017**, *29*, 1605148. [[CrossRef](#)]
29. Li, X.; Zhang, J.; Huo, Y.; Dai, K.; Li, S.; Chen, S. Two-dimensional sulfur- and chlorine-codoped g-C₃N₄/CdSe-amine heterostructures nanocomposite with effective interfacial charge transfer and mechanism insight. *Appl. Catal. B-Environ.* **2021**, *280*, 119452. [[CrossRef](#)]
30. Li, G.; Tang, Y.; Fu, T.; Xiang, Y.; Xiong, Z.; Si, Y.; Guo, C.; Jiang, Z. S, N co-doped carbon nanotubes coupled with CoFe nanoparticles as an efficient bifunctional ORR/OER electrocatalyst for rechargeable Zn-air batteries. *Chem. Eng. J.* **2022**, *429*, 132174. [[CrossRef](#)]
31. Yu, B.; Shi, J.; Tan, S.; Cui, Y.; Zhao, W.; Wu, H.; Luo, Y.; Li, D.; Meng, Q. Efficient (>20%) and Stable All-Inorganic Cesium Lead Triiodide Solar Cell Enabled by Thiocyanate Molten Salts. *Angew. Chem.-Int. Ed.* **2021**, *60*, 13436–13443. [[CrossRef](#)] [[PubMed](#)]
32. Su, Y.; Zhang, Y.; Zhuang, X.; Li, S.; Wu, D.; Zhang, F.; Feng, X. Low-temperature synthesis of nitrogen/sulfur co-doped three-dimensional graphene frameworks as efficient metal-free electrocatalyst for oxygen reduction reaction. *Carbon* **2013**, *62*, 296–301. [[CrossRef](#)]
33. Zhang, L.; Xu, Z. A review of current progress of recycling technologies for metals from waste electrical and electronic equipment. *J. Clean. Prod.* **2016**, *127*, 19–36. [[CrossRef](#)]
34. Ye, C.; Li, J.-X.; Li, Z.-J.; Li, X.-B.; Fan, X.-B.; Zhang, L.-P.; Chen, B.; Tung, C.-H.; Wu, L.-Z. Enhanced Driving Force and Charge Separation Efficiency of Protonated g-C₃N₄ for Photocatalytic O₂ Evolution. *ACS Catal.* **2015**, *5*, 6973–6979. [[CrossRef](#)]
35. Zhang, G.; Zang, S.; Wang, X. Layered Co(OH)(2) Deposited Polymeric Carbon Nitrides for Photocatalytic Water Oxidation. *ACS Catal.* **2015**, *5*, 941–947. [[CrossRef](#)]
36. Hao, X.; Zhou, J.; Cui, Z.; Wang, Y.; Wang, Y.; Zou, Z. Zn-vacancy mediated electron-hole separation in ZnS/g-C₃N₄ heterojunction for efficient visible-light photocatalytic hydrogen production. *Appl. Catal. B-Environ.* **2018**, *229*, 41–51. [[CrossRef](#)]
37. Tang, J.-Y.; Guo, R.-T.; Zhou, W.-G.; Huang, C.-Y.; Pan, W.-G. Ball-flower like NiO/g-C₃N₄ heterojunction for efficient visible light photocatalytic CO₂ reduction. *Appl. Catal. B-Environ.* **2018**, *237*, 802–810. [[CrossRef](#)]
38. Zhang, H.; Zhao, L.; Geng, F.; Guo, L.-H.; Wan, B.; Yang, Y. Carbon dots decorated graphitic carbon nitride as an efficient metal-free photocatalyst for phenol degradation. *Appl. Catal. B-Environ.* **2016**, *180*, 656–662. [[CrossRef](#)]
39. Wang, Z.; Guan, W.; Sun, Y.; Dong, F.; Zhou, Y.; Ho, W.-K. Water-assisted production of honeycomb-like g-C₃N₄ with ultralong carrier lifetime and outstanding photocatalytic activity. *Nanoscale* **2015**, *7*, 2471–2479. [[CrossRef](#)]
40. Goettmann, F.; Fischer, A.; Antonietti, M.; Thomas, A. Metal-free catalysis of sustainable Friedel-Crafts reactions: Direct activation of benzene by carbon nitrides to avoid the use of metal chlorides and halogenated compounds. *Chem. Commun.* **2006**, 4530–4532. [[CrossRef](#)]
41. Niu, Y.; Hu, F.; Xu, H.; Zhang, S.; Song, B.; Wang, H.; Li, M.; Shao, G.; Wang, H.; Lu, H. Exploration for high performance g-C₃N₄ photocatalyst from different precursors. *Mater. Today Commun.* **2023**, *34*, 105040. [[CrossRef](#)]
42. Thi Kim Anh, N.; Thanh-Truc, P.; Huy, N.-P.; Shin, E.W. The effect of graphitic carbon nitride precursors on the photocatalytic dye degradation of water-dispersible graphitic carbon nitride photocatalysts. *Appl. Surf. Sci.* **2021**, *537*, 148027.
43. Cardenas, A.; Vazquez, A.; Obregon, S.; Ruiz-Gomez, M.A.; Rodriguez-Gonzalez, V. New insights into the fluorescent sensing of Fe³⁺ ions by g-C₃N₄ prepared from different precursors. *Mater. Res. Bull.* **2021**, *142*, 111385. [[CrossRef](#)]
44. Liu, X.; Xu, X.; Gan, H.; Yu, M.; Huang, Y. The Effect of Different g-C₃N₄ Precursor Nature on Its Structural Control and Photocatalytic Degradation Activity. *Catalysts* **2023**, *13*, 848. [[CrossRef](#)]
45. Catherine, H.N.; Chiu, W.-L.; Chang, L.-L.; Tung, K.-L.; Hu, C. Gel-like Ag-Dicyandiamide Metal-Organic Supramolecular Network-Derived g-C₃N₄ for Photocatalytic Hydrogen Generation. *Acs Sustain. Chem. Eng.* **2022**, *10*, 8360–8369. [[CrossRef](#)]
46. Ren, X.; Yu, Q.; Pan, J.; Wang, Q.; Li, Y.; Shi, N. Photocatalytic degradation of methylene blue by C/g-C₃N₄ composites formed by different carbon sources. *React. Kinet. Mech. Catal.* **2022**, *135*, 2279–2289. [[CrossRef](#)]
47. Wang, X.; Maeda, K.; Thomas, A.; Takanabe, K.; Xin, G.; Carlsson, J.M.; Domen, K.; Antonietti, M. A metal-free polymeric photocatalyst for hydrogen production from water under visible light. *Nat. Mater.* **2009**, *8*, 76–80. [[CrossRef](#)] [[PubMed](#)]
48. Ang, T.P.; Chan, Y.M. Comparison of the Melon Nanocomposites in Structural Properties and Photocatalytic Activities. *J. Phys. Chem. C* **2011**, *115*, 15965–15972. [[CrossRef](#)]
49. Zhang, G.; Zhang, J.; Zhang, M.; Wang, X. Polycondensation of thiourea into carbon nitride semiconductors as visible light photocatalysts. *J. Mater. Chem.* **2012**, *22*, 8083–8091. [[CrossRef](#)]
50. Xiao, H.; Wang, W.; Liu, G.; Chen, Z.; Lv, K.; Zhu, J. Photocatalytic performances of g-C₃N₄ based catalysts for RhB degradation: Effect of preparation conditions. *Appl. Surf. Sci.* **2015**, *358*, 313–318. [[CrossRef](#)]
51. Sun, T.; Li, C.; Bao, Y.; Fan, J.; Liu, E. S-Scheme MnCo₂S₄/g-C₃N₄ Heterojunction Photocatalyst for H₂ Production. *Acta Phys.-Chim. Sin.* **2023**, *39*, 2212009. [[CrossRef](#)]

52. Wang, J.; Wang, S. A critical review on graphitic carbon nitride (g-C₃N₄)-based materials: Preparation, modification and environmental application. *Coord. Chem. Rev.* **2022**, *453*, 214338. [[CrossRef](#)]
53. Zhang, X.; Ma, P.; Wang, C.; Gan, L.; Chen, X.; Zhang, P.; Wang, Y.; Li, H.; Wang, L.; Zhou, X.; et al. Unraveling the dual defect sites in graphite carbon nitride for ultra-high photocatalytic H₂O₂ evolution. *Energy Environ. Sci.* **2022**, *15*, 830–842. [[CrossRef](#)]
54. Baladi, E.; Davar, F.; Hojjati-Najafabadi, A. Synthesis and characterization of g-C₃N₄-CoFe₂O₄-ZnO magnetic nanocomposites for enhancing photocatalytic activity with visible light for degradation of penicillin G antibiotic. *Environ. Res.* **2022**, *215*, 114270. [[CrossRef](#)] [[PubMed](#)]
55. Yan, S.C.; Li, Z.S.; Zou, Z.G. Photodegradation Performance of g-C₃N₄ Fabricated by Directly Heating Melamine. *Langmuir* **2009**, *25*, 10397–10401. [[CrossRef](#)] [[PubMed](#)]
56. Zhang, Y.; Liu, J.; Wu, G.; Chen, W. Porous graphitic carbon nitride synthesized via direct polymerization of urea for efficient sunlight-driven photocatalytic hydrogen production. *Nanoscale* **2012**, *4*, 5300–5303. [[CrossRef](#)] [[PubMed](#)]
57. Cui, Y.; Zhang, G.; Lin, Z.; Wang, X. Condensed and low-defected graphitic carbon nitride with enhanced photocatalytic hydrogen evolution under visible light irradiation. *Appl. Catal. B-Environ.* **2016**, *181*, 413–419. [[CrossRef](#)]
58. Xu, Q.; Zhu, B.; Cheng, B.; Yu, J.; Zhou, M.; Ho, W. Photocatalytic H₂ evolution on graphdiyne/g-C₃N₄ hybrid nanocomposites. *Appl. Catal. B-Environ.* **2019**, *255*, 117770. [[CrossRef](#)]
59. Yan, H.; Chen, Y.; Xu, S. Synthesis of graphitic carbon nitride by directly heating sulfuric acid treated melamine for enhanced photocatalytic H₂ production from water under visible light. *Int. J. Hydrogen Energy* **2012**, *37*, 125–133. [[CrossRef](#)]
60. Dong, G.; Zhang, L. Porous structure dependent photoreactivity of graphitic carbon nitride under visible light. *J. Mater. Chem.* **2012**, *22*, 1160–1166. [[CrossRef](#)]
61. Zhang, X.-S.; Hu, J.-Y.; Jiang, H. Facile modification of a graphitic carbon nitride catalyst to improve its photoreactivity under visible light irradiation. *Chem. Eng. J.* **2014**, *256*, 230–237. [[CrossRef](#)]
62. Gao, J.; Zhou, Y.; Li, Z.; Yan, S.; Wang, N.; Zou, Z. High-yield synthesis of millimetre-long, semiconducting carbon nitride nanotubes with intense photoluminescence emission and reproducible photoconductivity. *Nanoscale* **2012**, *4*, 3687–3692. [[CrossRef](#)] [[PubMed](#)]
63. Zhong, Y.; Wang, Z.; Feng, J.; Yan, S.; Zhang, H.; Li, Z.; Zou, Z. Improvement in photocatalytic H₂ evolution over g-C₃N₄ prepared from protonated melamine. *Appl. Surf. Sci.* **2014**, *295*, 253–259. [[CrossRef](#)]
64. Zhang, J.; Sun, J.; Maeda, K.; Domen, K.; Liu, P.; Antonietti, M.; Fu, X.; Wang, X. Sulfur-mediated synthesis of carbon nitride: Band-gap engineering and improved functions for photocatalysis. *Energy Environ. Sci.* **2011**, *4*, 675–678. [[CrossRef](#)]
65. Zhang, J.; Zhang, M.; Zhang, G.; Wang, X. Synthesis of Carbon Nitride Semiconductors in Sulfur Flux for Water Photoredox Catalysis. *Acs Catal.* **2012**, *2*, 940–948. [[CrossRef](#)]
66. Gong, X.-Q.; Selloni, A.; Batzill, M.; Diebold, U. Steps on anatase TiO₂(101). *Nat. Mater.* **2006**, *5*, 665–670. [[CrossRef](#)] [[PubMed](#)]
67. Nowotny, M.K.; Sheppard, L.R.; Bak, T.; Nowotny, J. Defect chemistry of titanium dioxide. application of defect engineering in processing of TiO₂-based photocatalysts. *J. Phys. Chem. C* **2008**, *112*, 5275–5300. [[CrossRef](#)]
68. Hong, Z.; Shen, B.; Chen, Y.; Lin, B.; Gao, B. Enhancement of photocatalytic H₂ evolution over nitrogen-deficient graphitic carbon nitride. *J. Mater. Chem. A* **2013**, *1*, 11754–11761. [[CrossRef](#)]
69. Lau, V.W.-H.; Mesch, M.B.; Duppel, V.; Blum, V.; Senker, J.; Lotsch, B.V. Low-Molecular-Weight Carbon Nitrides for Solar Hydrogen Evolution. *J. Am. Chem. Soc.* **2015**, *137*, 1064–1072. [[CrossRef](#)]
70. Niu, P.; Liu, G.; Cheng, H.-M. Nitrogen Vacancy-Promoted Photocatalytic Activity of Graphitic Carbon Nitride. *J. Phys. Chem. C* **2012**, *116*, 11013–11018. [[CrossRef](#)]
71. Niu, P.; Yin, L.-C.; Yang, Y.-Q.; Liu, G.; Cheng, H.-M. Increasing the Visible Light Absorption of Graphitic Carbon Nitride (Melon) Photocatalysts by Homogeneous Self-Modification with Nitrogen Vacancies. *Adv. Mater.* **2014**, *26*, 8046–8052. [[CrossRef](#)] [[PubMed](#)]
72. Martin, D.J.; Qiu, K.; Shevlin, S.A.; Handoko, A.D.; Chen, X.; Guo, Z.; Tang, J. Highly Efficient Photocatalytic H₂ Evolution from Water using Visible Light and Structure-Controlled Graphitic Carbon Nitride. *Angew. Chem.-Int. Ed.* **2014**, *53*, 9240–9245. [[CrossRef](#)] [[PubMed](#)]
73. Tay, Q.; Kanhere, P.; Ng, C.F.; Chen, S.; Chakraborty, S.; Huan, A.C.H.; Sum, T.C.; Ahuja, R.; Chen, Z. Defect Engineered g-C₃N₄ for Efficient Visible Light Photocatalytic Hydrogen Production. *Chem. Mater.* **2015**, *27*, 4930–4933. [[CrossRef](#)]
74. Mo, Z.; She, X.; Li, Y.; Liu, L.; Huang, L.; Chen, Z.; Zhang, Q.; Xu, H.; Li, H. Synthesis of g-C₃N₄ at different temperatures for superior visible/UV photocatalytic performance and photoelectrochemical sensing of MB solution. *Rsc Adv.* **2015**, *5*, 101552–101562. [[CrossRef](#)]
75. Dong, G.; Ho, W.; Wang, C. Selective photocatalytic N₂ fixation dependent on g-C₃N₄ induced by nitrogen vacancies. *J. Mater. Chem. A* **2015**, *3*, 23435–23441. [[CrossRef](#)]
76. Wu, G.; Thind, S.S.; Wen, J.; Yan, K.; Chen, A. A novel nanoporous α-C₃N₄ photocatalyst with superior high visible light activity. *Appl. Catal. B-Environ.* **2013**, *142*, 590–597. [[CrossRef](#)]
77. Liu, J.; Wang, H.; Chen, Z.P.; Moehwald, H.; Fiechter, S.; van de Krol, R.; Wen, L.; Jiang, L.; Antonietti, M. Microcontact-Printing-Assisted Access of Graphitic Carbon Nitride Films with Favorable Textures toward Photoelectrochemical Application. *Adv. Mater.* **2015**, *27*, 712–718. [[CrossRef](#)] [[PubMed](#)]
78. Yang, Z.; Zhang, Y.; Schnepf, Z. Soft and hard templating of graphitic carbon nitride. *J. Mater. Chem. A* **2015**, *3*, 14081–14092. [[CrossRef](#)]

79. Tong, Z.; Yang, D.; Li, Z.; Nan, Y.; Ding, F.; Shen, Y.; Jiang, Z. Thylakoid-Inspired Multishell g-C₃N₄ Nanocapsules with Enhanced Visible-Light Harvesting and Electron Transfer Properties for High-Efficiency Photocatalysis. *ACS Nano* **2017**, *11*, 1103–1112. [[CrossRef](#)]
80. Ong, W.-J.; Tan, L.-L.; Ng, Y.H.; Yong, S.-T.; Chai, S.-P. Graphitic Carbon Nitride (g-C₃N₄)-Based Photocatalysts for Artificial Photosynthesis and Environmental Remediation: Are We a Step Closer To Achieving Sustainability? *Chem. Rev.* **2016**, *116*, 7159–7329. [[CrossRef](#)]
81. Dong, G.; Zhang, Y.; Pan, Q.; Qiu, J. A fantastic graphitic carbon nitride (g-C₃N₄) material: Electronic structure, photocatalytic and photoelectronic properties. *J. Photochem. Photobiol. C-Photochem. Rev.* **2014**, *20*, 33–50. [[CrossRef](#)]
82. Li, M.; Zhang, L.; Wu, M.; Du, Y.; Fan, X.; Wang, M.; Zhang, L.; Kong, Q.; Shi, J. Mesoporous CeO₂/g-C₃N₄ nanocomposites: Remarkably enhanced photocatalytic activity for CO₂ reduction by mutual component activations. *Nano Energy* **2016**, *19*, 145–155. [[CrossRef](#)]
83. Dong, J.; Zhang, Y.; Hussain, M.I.; Zhou, W.; Chen, Y.; Wang, L.-N. g-C₃N₄: Properties, Pore Modifications, and Photocatalytic Applications. *Nanomaterials* **2022**, *12*, 121. [[CrossRef](#)] [[PubMed](#)]
84. Zhao, S.; Zhang, Y.; Zhou, Y.; Wang, Y.; Qiu, K.; Zhang, C.; Fang, J.; Sheng, X. Facile one-step synthesis of hollow mesoporous g-C₃N₄ spheres with ultrathin nanosheets for photoredox water splitting. *Carbon* **2018**, *126*, 247–256. [[CrossRef](#)]
85. Hu, R.; Wang, X.; Dai, S.; Shao, D.; Hayat, T.; Alsaedi, A. Application of graphitic carbon nitride for the removal of Pb(II) and aniline from aqueous solutions. *Chem. Eng. J.* **2015**, *260*, 469–477. [[CrossRef](#)]
86. Fukasawa, Y.; Takanebe, K.; Shimojima, A.; Antonietti, M.; Domen, K.; Okubo, T. Synthesis of Ordered Porous Graphitic-C₃N₄ and Regularly Arranged Ta₃N₅ Nanoparticles by Using Self-Assembled Silica Nanospheres as a Primary Template. *Chem. Asian J.* **2011**, *6*, 103–109. [[CrossRef](#)] [[PubMed](#)]
87. Chen, X.; Wang, H.; Meng, R.; Chen, M. Porous Graphitic Carbon Nitride Synthesized via Using Carbon Nanotube as a Novel Recyclable Hard Template for Efficient Visible Light Photocatalytic Organic Pollutant Degradation. *Chemistryselect* **2019**, *4*, 6123–6129. [[CrossRef](#)]
88. Zhang, Y.; Schnepf, Z.; Cao, J.; Ouyang, S.; Li, Y.; Ye, J.; Liu, S. Biopolymer-Activated Graphitic Carbon Nitride towards a Sustainable Photocathode Material. *Sci. Rep.* **2013**, *3*, 2163. [[CrossRef](#)]
89. Xu, J.; Wang, Y.; Zhu, Y. Nanoporous Graphitic Carbon Nitride with Enhanced Photocatalytic Performance. *Langmuir* **2013**, *29*, 10566–10572. [[CrossRef](#)]
90. Wang, Y.; Wang, X.; Antonietti, M.; Zhang, Y. Facile One-Pot Synthesis of Nanoporous Carbon Nitride Solids by Using Soft Templates. *ChemSuschem* **2010**, *3*, 435–439. [[CrossRef](#)]
91. Shen, W.; Ren, L.; Zhou, H.; Zhang, S.; Fan, W. Facile one-pot synthesis of bimodal mesoporous carbon nitride and its function as a lipase immobilization support. *J. Mater. Chem.* **2011**, *21*, 3890–3894. [[CrossRef](#)]
92. Shalom, M.; Inal, S.; Fettkenhauer, C.; Neher, D.; Antonietti, M. Improving Carbon Nitride Photocatalysis by Supramolecular Preorganization of Monomers. *J. Am. Chem. Soc.* **2013**, *135*, 7118–7121. [[CrossRef](#)] [[PubMed](#)]
93. Zhang, M.; Yan, X.; Huang, F.; Niu, Z.; Gibson, H.W. Stimuli-Responsive Host-Guest Systems Based on the Recognition of Cryptands by Organic Guests. *Acc. Chem. Res.* **2014**, *47*, 1995–2005. [[CrossRef](#)] [[PubMed](#)]
94. Cui, Q.; Xu, J.; Wang, X.; Li, L.; Antonietti, M.; Shalom, M. Phenyl-Modified Carbon Nitride Quantum Dots with Distinct Photoluminescence Behavior. *Angew. Chem.-Int. Ed.* **2016**, *55*, 3672–3676. [[CrossRef](#)] [[PubMed](#)]
95. Bhunia, M.K.; Yamauchi, K.; Takanebe, K. Harvesting Solar Light with Crystalline Carbon Nitrides for Efficient Photocatalytic Hydrogen Evolution. *Angew. Chem.-Int. Ed.* **2014**, *53*, 11001–11005. [[CrossRef](#)] [[PubMed](#)]
96. Jordan, T.; Fechner, N.; Xu, J.; Brenner, T.J.K.; Antonietti, M.; Shalom, M. “Caffeine Doping” of Carbon/Nitrogen-Based Organic Catalysts: Caffeine as a Supramolecular Edge Modifier for the Synthesis of Photoactive Carbon Nitride Tubes. *Chemcatchem* **2015**, *7*, 2826–2830. [[CrossRef](#)]
97. Gao, J.; Wang, J.; Qian, X.; Dong, Y.; Xu, H.; Song, R.; Yan, C.; Zhu, H.; Zhong, Q.; Qian, G.; et al. One-pot synthesis of copper-doped graphitic carbon nitride nanosheet by heating Cu-melamine supramolecular network and its enhanced visible-light-driven photocatalysis. *J. Solid State Chem.* **2015**, *228*, 60–64. [[CrossRef](#)]
98. Chen, Z.P.; Antonietti, M.; Dontsova, D. Enhancement of the Photocatalytic Activity of Carbon Nitrides by Complex Templating. *Chem. A Eur. J.* **2015**, *21*, 10805–10811. [[CrossRef](#)]
99. Shalom, M.; Guttentag, M.; Fettkenhauer, C.; Inal, S.; Neher, D.; Llobet, A.; Antonietti, M. In Situ Formation of Heterojunctions in Modified Graphitic Carbon Nitride: Synthesis and Noble Metal Free Photocatalysis. *Chem. Mater.* **2014**, *26*, 5812–5818. [[CrossRef](#)]
100. Fan, X.; Xing, Z.; Shu, Z.; Zhang, L.; Wang, L.; Shi, J. Improved photocatalytic activity of g-C₃N₄ derived from cyanamide-urea solution. *RSC Adv.* **2015**, *5*, 8323–8328. [[CrossRef](#)]
101. Shalom, M.; Gimenez, S.; Schipper, F.; Herraiz-Cardona, I.; Bisquert, J.; Antonietti, M. Controlled Carbon Nitride Growth on Surfaces for Hydrogen Evolution Electrodes. *Angew. Chem.-Int. Ed.* **2014**, *53*, 3654–3658. [[CrossRef](#)] [[PubMed](#)]
102. Jun, Y.-S.; Lee, E.Z.; Wang, X.; Hong, W.H.; Stucky, G.D.; Thomas, A. From Melamine-Cyanuric Acid Supramolecular Aggregates to Carbon Nitride Hollow Spheres. *Adv. Funct. Mater.* **2013**, *23*, 3661–3667. [[CrossRef](#)]
103. Bai, X.; Wang, L.; Zong, R.; Zhu, Y. Photocatalytic Activity Enhanced via g-C₃N₄ Nanoplates to Nanorods. *J. Phys. Chem. C* **2013**, *117*, 9952–9961. [[CrossRef](#)]
104. Wang, S.; Li, C.; Wang, T.; Zhang, P.; Li, A.; Gong, J. Controllable synthesis of nanotube-type graphitic C₃N₄ and their visible-light photocatalytic and fluorescent properties. *J. Mater. Chem. A* **2014**, *2*, 2885–2890. [[CrossRef](#)]

105. Chen, D.; Wang, K.; Xiang, D.; Zong, R.; Yao, W.; Zhu, Y. Significantly enhancement of photocatalytic performances via core-shell structure of ZnO@mpg-C₃N₄. *Appl. Catal. B-Environ.* **2014**, *147*, 554–561. [[CrossRef](#)]
106. Cheng, F.; Wang, H.; Dong, X. The amphoteric properties of g-C₃N₄ nanosheets and fabrication of their relevant heterostructure photocatalysts by an electrostatic re-assembly route. *Chem. Commun.* **2015**, *51*, 7176–7179. [[CrossRef](#)] [[PubMed](#)]
107. Schwinghammer, K.; Mesch, M.B.; Duppel, V.; Ziegler, C.; Senker, J.; Lotsch, B.V. Crystalline Carbon Nitride Nanosheets for Improved Visible-Light Hydrogen Evolution. *J. Am. Chem. Soc.* **2014**, *136*, 1730–1733. [[CrossRef](#)] [[PubMed](#)]
108. Liu, G.; Wang, T.; Zhang, H.; Meng, X.; Hao, D.; Chang, K.; Li, P.; Kako, T.; Ye, J. Nature-Inspired Environmental “Phosphorylation” Boosts Photocatalytic H₂ Production over Carbon Nitride Nanosheets under Visible-Light Irradiation. *Angew. Chem.-Int. Ed.* **2015**, *54*, 13561–13565. [[CrossRef](#)]
109. Niu, P.; Zhang, L.; Liu, G.; Cheng, H.-M. Graphene-Like Carbon Nitride Nanosheets for Improved Photocatalytic Activities. *Adv. Funct. Mater.* **2012**, *22*, 4763–4770. [[CrossRef](#)]
110. Yang, S.; Gong, Y.; Zhang, J.; Zhan, L.; Ma, L.; Fang, Z.; Vajtai, R.; Wang, X.; Ajayan, P.M. Exfoliated Graphitic Carbon Nitride Nanosheets as Efficient Catalysts for Hydrogen Evolution under Visible Light. *Adv. Mater.* **2013**, *25*, 2452–2456. [[CrossRef](#)]
111. Zhao, H.; Yu, H.; Quan, X.; Chen, S.; Zhang, Y.; Zhao, H.; Wang, H. Fabrication of atomic single layer graphitic-C₃N₄ and its high performance of photocatalytic disinfection under visible light irradiation. *Appl. Catal. B-Environ.* **2014**, *152*, 46–50. [[CrossRef](#)]
112. Yin, Y.; Han, J.; Zhang, X.; Zhang, Y.; Zhou, J.; Muir, D.; Sutarto, R.; Zhang, Z.; Liu, S.; Song, B. Facile synthesis of few-layer-thick carbon nitride nanosheets by liquid ammonia-assisted lithiation method and their photocatalytic redox properties. *RSC Adv.* **2014**, *4*, 32690–32697. [[CrossRef](#)]
113. Ma, L.; Fan, H.; Li, M.; Tian, H.; Fang, J.; Dong, G. A simple melamine-assisted exfoliation of polymeric graphitic carbon nitrides for highly efficient hydrogen production from water under visible light. *J. Mater. Chem. A* **2015**, *3*, 22404–22412. [[CrossRef](#)]
114. Xu, H.; Yan, J.; She, X.; Xu, L.; Xia, J.; Xu, Y.; Song, Y.; Huang, L.; Li, H. Graphene-analogue carbon nitride: Novel exfoliation synthesis and its application in photocatalysis and photoelectrochemical selective detection of trace amount of Cu²⁺. *Nanoscale* **2014**, *6*, 1406–1415. [[CrossRef](#)] [[PubMed](#)]
115. Ma, L.; Fan, H.; Wang, J.; Zhao, Y.; Tian, H.; Dong, G. Water-assisted ions in situ intercalation for porous polymeric graphitic carbon nitride nanosheets with superior photocatalytic hydrogen evolution performance. *Appl. Catal. B Environ.* **2016**, *190*, 93–102. [[CrossRef](#)]
116. Zhou, L.; Zhang, H.; Sun, H.; Liu, S.; Tade, M.O.; Wang, S.; Jin, W. Recent advances in non-metal modification of graphitic carbon nitride for photocatalysis: A historic review. *Catal. Sci. Technol.* **2016**, *6*, 7002–7023. [[CrossRef](#)]
117. Zhou, L.; Feng, J.; Qiu, B.; Zhou, Y.; Lei, J.; Xing, M.; Wang, L.; Zhou, Y.; Liu, Y.; Zhang, J. Ultrathin g-C₃N₄ nanosheet with hierarchical pores and desirable energy band for highly efficient H₂O₂ production. *Appl. Catal. B-Environ.* **2020**, *267*, 118396. [[CrossRef](#)]
118. Tang, C.; Cheng, M.; Lai, C.; Li, L.; Yang, X.; Du, L.; Zhang, G.; Wang, G.; Yang, L. Recent progress in the applications of non-metal modified graphitic carbon nitride in photocatalysis. *Coord. Chem. Rev.* **2023**, *474*, 214846. [[CrossRef](#)]
119. Sudhaik, A.; Raizada, P.; Shandilya, P.; Jeong, D.-Y.; Lim, J.-H.; Singh, P. Review on fabrication of graphitic carbon nitride based efficient nanocomposites for photodegradation of aqueous phase organic pollutants. *J. Ind. Eng. Chem.* **2018**, *67*, 28–51. [[CrossRef](#)]
120. Nasir, M.S.; Yang, G.; Ayub, I.; Wang, S.; Wang, L.; Wang, X.; Yan, W.; Peng, S.; Ramakarishna, S. Recent development in graphitic carbon nitride based photocatalysis for hydrogen generation. *Appl. Catal. B-Environ.* **2019**, *257*, 117855. [[CrossRef](#)]
121. Hayat, A.; Syed, J.A.S.G.; Al-Sehemi, A.S.; El-Nasser, K.; Taha, T.A.A.; Al-Ghamdi, A.A.; Amin, M.; Ajmal, Z.; Iqbal, W.; Palamanit, A.; et al. State of the art advancement in rational design of g-C₃N₄ photocatalyst for efficient solar fuel transformation, environmental decontamination and future perspectives. *Int. J. Hydrogen Energy* **2022**, *47*, 10837–10867. [[CrossRef](#)]
122. Zeng, Y.; Liu, X.; Liu, C.; Wang, L.; Xia, Y.; Zhang, S.; Luo, S.; Pei, Y. Scalable one-step production of porous oxygen-doped g-C₃N₄ nanorods with effective electron separation for excellent visible-light photocatalytic activity. *Appl. Catal. B-Environ.* **2018**, *224*, 1–9. [[CrossRef](#)]
123. Liu, Q.; Zhang, J. Graphene Supported Co-g-C₃N₄ as a Novel Metal-Macrocylic Electrocatalyst for the Oxygen Reduction Reaction in Fuel Cells. *Langmuir* **2013**, *29*, 3821–3828. [[CrossRef](#)] [[PubMed](#)]
124. Jiang, J.; Cao, S.; Hu, C.; Chen, C. A comparison study of alkali metal-doped g-C₃N₄ for visible-light photocatalytic hydrogen evolution. *Chin. J. Catal.* **2017**, *38*, 1981–1989. [[CrossRef](#)]
125. He, F.; Wang, Z.; Li, Y.; Peng, S.; Liu, B. The nonmetal modulation of composition and morphology of g-C₃N₄-based photocatalysts. *Appl. Catal. B-Environ.* **2020**, *269*, 118828. [[CrossRef](#)]
126. Gong, Y.; Zhao, X.; Zhang, H.; Yang, B.; Xiao, K.; Guo, T.; Zhang, J.; Shao, H.; Wang, Y.; Yu, G. MOF-derived nitrogen doped carbon modified g-C₃N₄ heterostructure composite with enhanced photocatalytic activity for bisphenol A degradation with peroxydisulfate under visible light irradiation. *Appl. Catal. B-Environ.* **2018**, *233*, 35–45. [[CrossRef](#)]
127. Cao, S.; Low, J.; Yu, J.; Jaroniec, M. Polymeric Photocatalysts Based on Graphitic Carbon Nitride. *Adv. Mater.* **2015**, *27*, 2150–2176. [[CrossRef](#)] [[PubMed](#)]
128. Xiong, T.; Cen, W.; Zhang, Y.; Dong, F. Bridging the g-C₃N₄ Interlayers for Enhanced Photocatalysis. *Acs Catal.* **2016**, *6*, 2462–2472. [[CrossRef](#)]
129. Wen, J.; Zhou, L.; Tang, Q.; Xiao, X.; Sun, S. Photocatalytic degradation of organic pollutants by carbon quantum dots functionalized g-C₃N₄: A review. *Ecotoxicol. Environ. Saf.* **2023**, *262*, 115133. [[CrossRef](#)]

130. Wang, Y.; Zhong, S.; Niu, Z.; Dai, Y.; Li, J. Synthesis and up-to-date applications of 2D microporous g-C₃N₄ nanomaterials for sustainable development. *Chem. Commun.* **2023**, *59*, 10883–10911. [[CrossRef](#)]
131. Truong, H.B.; Hur, J.; Nguyen, X.C. Recent advances in g-C₃N₄-based photocatalysis for water treatment: Magnetic and floating photocatalysts, and applications of machine-learning techniques. *J. Environ. Manag.* **2023**, *345*, 118895. [[CrossRef](#)]
132. Ding, M.; Wei, Z.; Zhu, X.; Liu, D. Effect of Different g-C₃N₄ Content on Properties of NiCo₂S₄/g-C₃N₄ Composite as Electrode Material for Supercapacitor. *Int. J. Electrochem. Sci.* **2022**, *17*, 22121. [[CrossRef](#)]
133. Chen, X.; Shi, R.; Chen, Q.; Zhang, Z.; Jiang, W.; Zhu, Y.; Zhang, T. Three-dimensional porous g-C₃N₄ for highly efficient photocatalytic overall water splitting. *Nano Energy* **2019**, *59*, 644–650. [[CrossRef](#)]
134. Fu, J.; Zhu, B.; Jiang, C.; Cheng, B.; You, W.; Yu, J. Hierarchical Porous O-Doped g-C₃N₄ with Enhanced Photocatalytic CO₂ Reduction Activity. *Small* **2017**, *13*, 1603938. [[CrossRef](#)]
135. Dou, M.; Wang, J.; Gao, B.; Xu, C.; Yang, F. Photocatalytic difference of amoxicillin and cefotaxime under visible light by mesoporous g-C₃N₄: Mechanism, degradation pathway and DFT calculation. *Chem. Eng. J.* **2020**, *383*, 123134. [[CrossRef](#)]

Disclaimer/Publisher's Note: The statements, opinions and data contained in all publications are solely those of the individual author(s) and contributor(s) and not of MDPI and/or the editor(s). MDPI and/or the editor(s) disclaim responsibility for any injury to people or property resulting from any ideas, methods, instructions or products referred to in the content.